Cancer Science
Japanese Cancer Association JCA
Open Access

# Live imaging of transforming growth factor-β activated kinase 1 activation in Lewis lung carcinoma 3LL cells implanted into syngeneic mice and treated with polyinosinic:polycytidylic acid

**Saori Takaoka,[1] Yuji Kamioka,[1,2] Kanako Takakura,[3] Ai Baba,[4] Hiroaki Shime,[5] Tsukasa Seya[5] and Michiyuki Matsuda[1,4]**

[1]Department of Pathology and Biology of Diseases, Graduate School of Medicine; [2]Innovative Techno-Hub for Integrated Medical Bio-Imaging; [3]Imaging Platform for Spatio-Temporal Regulation, Graduate School of Medicine; [4]Laboratory of Bioimaging and Cell Signaling, Graduate School of Biostudies, Kyoto University, Kyoto; [5]Department of Microbiology and Immunology, Graduate School of Medicine, Hokkaido University, Sapporo, Japan

**Key words**

Förster (or fluorescence) resonance energy transfer, *in vivo* imaging, polyinosinic:polycytidylic acid (PolyI:C), TGF-β activated kinase 1, two-photon excitation microscopy

**Correspondence**

Yuji Kamioka, Department of Pathology and Biology of Diseases, Graduate School of Medicine, Kyoto University, Yoshidakonoe-cho, Sakyo-ku, Kyoto 606-8501, Japan.
Tel: +81-75-753-9450; Fax: +81-75-753-4698;
E-mail: ykamioka@lif.kyoto-u.ac.jp

**Funding Information**

Ministry of Education, Culture, Sports, and Science of Japan; Japan Agency for Medical Research and Development; Special Coordination Funds for Promoting Science and Technology; Japan Society for the Promotion of Science.

Received September 28, 2015; Revised February 1, 2016; Accepted February 28, 2016

*Cancer Sci* **107** (2016) 644–652

doi: 10.1111/cas.12923

**Transforming growth factor-β activated kinase 1 (TAK1) has been shown to play a crucial role in cell death, differentiation, and inflammation. Here, we live-imaged robust TAK1 activation in Lewis lung carcinoma 3LL cells implanted into the s.c. tissue of syngeneic C57BL/6 mice and treated with polyinosinic:polycytidylic acid (PolyI:C). First, we developed and characterized a Förster resonance energy transfer-based biosensor for TAK1 activity. The TAK1 biosensor, named Eevee-TAK1, responded to stress-inducing reagents such as anisomycin, tumor necrosis factor-α, and interleukin1-β. The anisomycin-induced increase in Förster resonance energy transfer was abolished by the TAK1 inhibitor (5z)-7-oxozeaenol. Activity of TAK1 in 3LL cells was markedly increased by PolyI:C in the presence of macrophages. 3LL cells expressing Eevee-TAK1 were implanted into mice and observed through imaging window by two-photon excitation microscopy. During the growth of tumor, the 3LL cells at the periphery of the tumor showed higher TAK1 activity than the 3LL cells located at the center of the tumor, suggesting that cells at the periphery of the tumor mass were under stronger stress. Injection of PolyI:C, which is known to induce regression of the implanted tumors, induced marked and homogenous TAK1 activation within the tumor tissues. The effect of PolyI:C faded within 4 days. These observations suggest that Eevee-TAK1 is a versatile tool to monitor cellular stress in cancer tissues.**

Transforming growth factor β-activated kinase 1 was first identified as a MAPK kinase downstream of TGF-β,[1] and has been shown to mediate Smad-independent TGF-β signaling to stress-responsive MAPK in a TRAF6-dependent manner, causing apoptosis and EMT.[2,3] Importantly, TAK1 also functions as a hub to transmit inflammatory signals elicited by IL-1β and TNF-α to the nuclear factor-κB pathway.[4,5] In the latter scenario, TAK1 prevents cells from apoptosis by multiple mechanisms.[6–8] The anti-apoptotic role of TAK1 has also been shown genetically: TAK1-deficient mice are embryonic lethal[9,10] or, in the case of conditional knockout, are suffering from dysfunction of the immune system or severe skin inflammation.[11,12] Recently, however, it has been revealed that prolonged TAK1 activation induces another type of cell death, necroptosis, adding further complexity to the known functions of TAK1 *in vivo*.[13]

Chronic inflammation contributes greatly to the generation of the tumor microenvironment, which includes a variety of cell types such as tumor-associated macrophages and myeloid-derived suppressor cells.[14,15] Pro-inflammatory cytokines such as TNF-α and IL-1β are the major players in fostering generation of the tumor microenvironment in chronic inflammation.[14,16] Accordingly, TAK1 has been shown to promote tumor growth in various ways. For example, TAK1 is essential for TNF-α-mediated metastasis of colon or breast cancer cells.[17,18] It is also required to inhibit apoptosis in KRas-transformed cells.[19] In this context, it is worth noting that tumor-associated macrophages and myeloid-derived suppressor cells have been shown to be converted into tumoricidal effectors by RNA adjuvant therapy, with TNF-α and IL-1β again acting as the major mediators.[20] Studies are therefore needed to determine how the inflammatory cytokine signaling pathway is regulated in an *in vivo* setting.

Genetically encoded biosensors based on fluorescent proteins and FRET have been developed in order to visualize the subcellular activities of signaling molecules.[21,22] Recent progress has enabled us to follow the activities of small GTPases and protein kinases for several days under a microscope, opening a

new window into the signal transduction of cancer cells.[23] For example, it has been shown that glioma cells exhibit marked heterogeneity in Rac1 activity and their levels of Rac1 activity have been correlated to their invasion capacities.[24] More recently, a FRET biosensor for ERK was used to investigate how melanoma cells build a niche to acquire drug tolerance.[25]

Here we report a novel FRET biosensor for TAK1 activity, called Eevee-TAK1, based on the optimized backbone.[26] Lewis lung carcinoma cells expressing Eevee-TAK1 were implanted s.c. into syngeneic mice and observed for 5 days through an imaging window by two-photon excitation microscopy. We found that TAK1 activity was higher at the invading front of the tumor tissues. Treatment with PolyI:C, which drives macrophages to secrete IL-1β and TNF-α, was found to evoke strong TAK1 activation diffusely in the tumor tissues. The combination of FRET biosensors and *in vivo* imaging will help us to untangle signaling pathways in living tissue.

## Materials and Methods

**Plasmids.** Construction and stable expression of the FRET biosensor were carried out as described previously.[26] The 3592NES FRET biosensor was based on the optimized Eevee backbone, which was comprised of the optimized fluorescent protein pair, YPet and ECFP, a long flexible EV-linker (116 a.a.), an FHA1 phospho-threonine-binding domain from yeast Rad53, a substrate sequence, and the NES from HIV-1 rev protein (LQLPPLERLTLD). The substrate sequence consisted of a.a. 276–295 of human cyclin D1 (EEEEEV-DLACTPT*D*VRDVDI), in which the +3 residue from the target phosphorylation site $Thr^{286}$ (underlined) was changed to an Asp (italicized) to increase affinity to the FHA1 domain. Stable cell lines expressing the 3592NES FRET biosensors were established by transposon-mediated gene transfer as described previously.[26,31] An expression vector for an active mutant of TAK1, TAK1-TAB, was kindly provided by Hiroaki Sakurai.[27] The plasmid was transfected into HeLa cells expressing 3592NES with 293fectin according to the manufacturer's protocol (Thermo Fisher Scientific, Waltham, MA, USA). The shRNA sequences inserted into pLKO.1-TRC are shown in Table 1.[28] Negative control vector containing scrambled shRNA (#1864) was purchased from Addgene (Cambridge, MA, USA). The 4T1 cells or 3LL cells were transfected with pLKO-shTAK1 #1–#5 or scramble control (scr) by Lipofectamine 3000 (Thermo Fisher Scientific), incubated for 2 days, and subjected to immunoblotting analysis or FRET imaging.

**Antibodies and reagents.** The following primary and secondary antibodies were used for immunoblotting analysis and immunocytochemistry: anti-TAK1 rabbit polyclonal antibody, anti-phospho-SAPK/JNK (Thr183/Tyr185) rabbit polyclonal antibody, and anti-phospho-p38 MAPK (Thr180/Tyr182) antibody (Cell Signaling Technology, Danvers, MA, USA); anti-TNF Receptor I rabbit polyclonal antibody (Abcam, Cambridge, UK); anti-IL-1 mouse mAb (Santa Cruz Biotechnology, Dallas, TX, USA); anti-α-tubulin (DM1A) mouse mAb (Merck Millipore, Billerica, MA, USA); IRDye 680 goat anti-mouse IgG and IRDye 800CW goat anti-rabbit (LI-COR Biosciences, Lincoln, NE, USA); and Alexa Fluor anti-mouse F4/80 antibody (BioLegend, San Diego, CA, USA). Mouse IL-1β and human TNF-α were from Wako (Osaka, Japan).

Blasticidin S and puromycin were purchased from InvivoGen (San Diego, CA). (5z)-7-oxozeaenol, JNK inhibitor VIII, anisomycin, dibutyryl cyclic AMP, and TPA were purchased from Merck Millipore. Epidermal growth factor, SB203580, IMD-0354, and PolyI:C were purchased from Sigma-Aldrich (St. Louis, MO, USA). The GSK-3β inhibitor, CHIR-99021, was purchased from Focus Biomolecules (Plymouth Meeting, PA, USA).

**Immunoblotting.** HeLa, 4T1, and 3LL cells were lysed in SDS sample buffer (62.5 mM Tris-HCl [pH 6.8], 12% glycerol, 2% SDS, 0.004% bromophenol blue and 5% 2-mercaptoethanol). After sonication, the samples were separated by SDS-PAGE and transferred to PVDF membranes (Merck Millipore). After blocking with Odyssey blocking buffer (LI-COR) for 30 min, the membranes were incubated with primary antibodies diluted in Can Get Signal (Toyobo, Osaka, Japan), followed by secondary antibodies diluted in Odyssey blocking buffer. Proteins were detected by an Odyssey Infrared scanner (LI-COR) and analyzed by using the Odyssey imaging software.

**Cell culture.** HeLa cells were purchased from the Human Science Research Resources Bank (Sennan-shi, Japan) and maintained in DMEM (Wako) containing 10% FBS (Sigma-Aldrich) and penicillin–streptomycin (Nacalai Tesque, Kyoto, Japan) at 37°C in a humidified atmosphere containing 5% $CO_2$.

Lewis lung carcinoma (3LL) cells were maintained in RPMI-1640 medium containing 10% FBS and penicillin–streptomycin at 37°C. 4T1 tumor cells were purchased from ATCC (Manassas, VA, USA) and cultured with RPMI-1640 medium containing 10% FBS and penicillin–streptomycin at 37°C.

**Preparation of macrophages.** Bone marrow cells were collected from 8 to 12-week-old C57BL/6 mice. Monocyte subsets were enriched by using an EasySep mouse monocyte enrichment kit (Stemcell Technologies, Vancouver, BC, Canada). Isolated monocytes were maintained in RPMI-1640 containing 10% FBS, penicillin–streptomycin, and 10% L929 cell-conditioned medium at 37°C in a humidified atmosphere containing 5% $CO_2$ on a UPCell dish (CellSeed, Tokyo, Japan). One to two weeks after isolation, monocytes proliferated and differentiated into macrophages, and were cocultured with 3LL cells expressing 3592NES.

**Epifluorescence microscopy of tissue culture cells.** Förster (or fluorescence) resonance energy transfer imaging with an inverted epifluorescence microscope was carried out essentially as described previously.[29] Cells were plated on 35-mm glass-base dishes, cultured for 24 h, and starved for 1 h in phenol red-free M199 (Thermo Fisher Scientific) containing 0.1% BSA. Cells were observed with an IX81 inverted microscope (Olympus, Tokyo, Japan) equipped with a UPlanSApo 40×/0.95 dry objective lens (Olympus), PlanApo 60×/1.40 oil objective lens (Olympus), a CoolSNAP K4 charge-coupled

**Table 1. shRNA sequences inserted into pLKO.1-TRC for TAK1 depletion**

| | |
|---|---|
| #1 | 5′-CCGGCTGAACCATTGCCTTACTACACTCTCGAGAGTGTAGTAAG GCAATGGTTCAGTTTTTG-3′ |
| #2 | 5′-CGGATGGACATTGCTTCTACAAATACCTCGAGGTATTTGTAGAA GCAATGTCCATTTTTTG-3′ |
| #3 | 5′-CCGGCAGGAGTATATGAAAGTTCAAACCTCGAGGTTTGAACTTT CATATACTCCTGTTTTTG-3′ |
| #4 | 5′-CCGGGAGAATTTGAACACTTACAAAGACTCGAGTCTTTGTAAGT GTTCAAATTCTCTTTTTG-3′ |
| #5 | 5′-CCGGAAGAGAATATTTATATTGTTAACCTCGAGGTTAACAATAT AAATATTCTCTTTTTTTG-3′ |

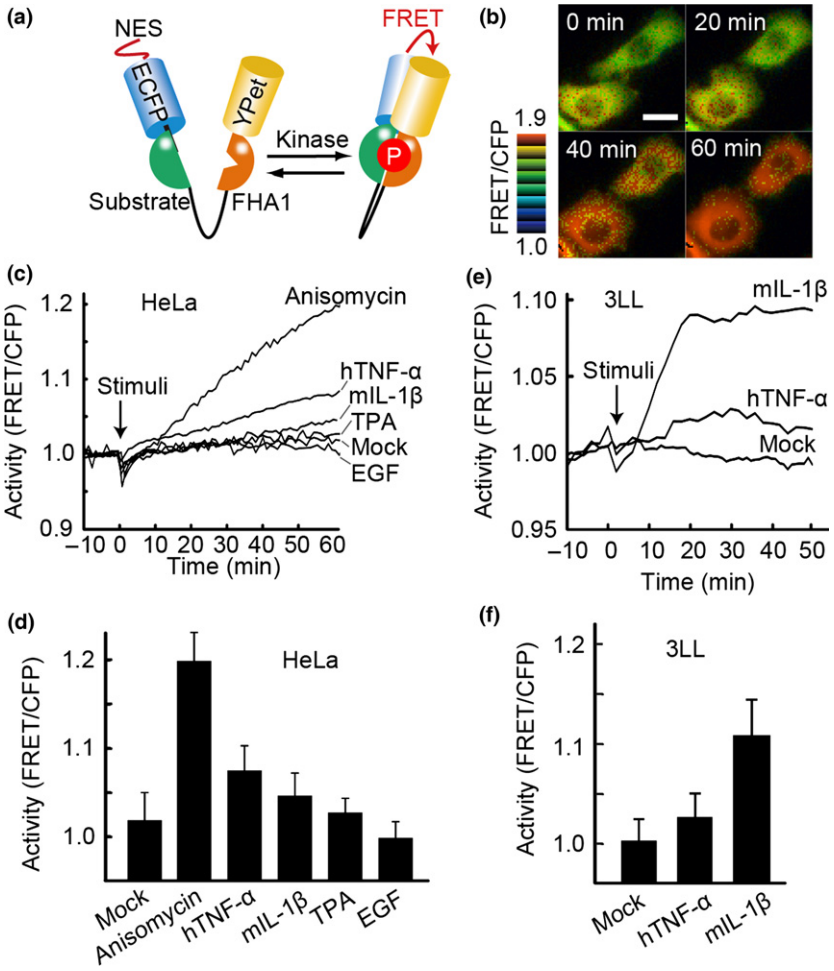


**Fig. 1.** Development and characterization of the 3592NES Förster resonance energy transfer (FRET) biosensor. (a) The 3592NES FRET biosensor comprised of a cyclin D1-derived substrate peptide and an FHA1 phospho-amino acid binding domain, sandwiched with fluorescent proteins YPet and ECFP. Phosphorylation of the substrate domain increases FRET. NES, nuclear export sequence. (b) HeLa cells expressing 3592NES were stimulated with 5 μg/mL anisomycin at 0 min. FRET/cyan fluorescent protein (CFP) images are depicted in the IMD display mode. Scale bar = 50 μm. (c,d) HeLa cells expressing 3592NES were stimulated with several stimuli-inducing reagents: 5 μg/mL anisomycin, 1 mM cyclic AMP (Mock), 1 μM TPA, 10 ng/mL epidermal growth factor (EGF), 270 ng/mL human tumor necrosis factor-α (hTNF-α), and 10 ng/mL mouse interleukin-1β (mIL-1β). (c) Representative time courses of FRET/CFP values. (d) Averages at 60 min of more than 20 cells under each condition from three independent experiments. (e) Lewis lung carcinoma 3LL cells expressing 3592NES were stimulated with 270 ng/mL TNF-α and 10 ng/mL IL-1β. (f) Representative time courses and averages at 60 min.

device camera (Roper Scientific, Tucson, AZ, USA), a CoolLED precisExcite LED illumination system (Molecular Devices, Sunnyvale, CA, USA), an IX2-ZDC laser-based auto-focusing system (Olympus), and an MD-XY30100T-Meta automatically programmable XY stage (SIGMA KOKI, Tokyo, Japan). Fluorescent images were acquired with the following filters purchased from Omega Optical (Brattleboro, VT, USA): an XF1071 440AF21 excitation filter, an XF2034 455DRLP dichroic mirror, and an XF3075 480AF30 emission filter for CFP, and a XF3079 535AF26 emission filter for FRET. Images were analyzed with Meta-Morph software (Universal Imaging, West Chester, PA, USA) as described previously.[29] Briefly, after background subtraction, FRET/CFP ratio images were generated in the intensity modulated display mode. For the time course analysis, fluorescent intensities were averaged over the whole cell area. The FRET/CFP values were averaged for 10 min before stimulation and used to normalize the changes in FRET/CFP values during observation.

**Mouse allograft model.** C57BL/6 mice were housed in a specific pathogen-free facility and received a routine chow diet and water *ad libitum*. Six to sixteen-week-old mice were used for the *in vivo* imaging. To prepare tumor-bearing mice, 3LL cells ($5 \times 10^6$ cells/30 μL PBS) were injected s.c. into the flank of mice. Tumors that reached to 150–1000 $mm^3$ (approximately 4 days after implantation) were observed under a two-photon excitation microscope. The animal protocols were reviewed and approved by the Animal Care and Use Committee of Kyoto University Graduate School of Medicine (No. 15064) (Kyoto, Japan).

***In vivo* observation through an imaging window.** The in-house-constructed imaging window consisted of a round coverslip (CO15001 Φ = 15 mm; Matsunami Glass Industry, Osaka, Japan) adhered to a ring-shaped magnet (Φ12 × Φ8.0 × 0.5 mm; Magfine Corp., Miyagi, Japan) with Aron Alpha (Toagosei, Tokyo, Japan). After shaving, the skin over the left femur region of a C57BL/6 mouse was incised for a span of 10 mm. The imaging window was inserted into the incision, which was then stitched with 6-0 nylon sutures (Ethicon, Cincinnati, OH, USA). After more than 1 week, a circular region of skin was removed to expose the imaging window. The 3LL cells expressing Eevee-TAK1 ($5 \times 10^6$ in PBS) were then injected beneath the imaging window. After 4–7 days, mice were anesthetized with 1.5–2% isoflurane (Abbot, Abbott Park, IL, USA) inhalation and placed in the prone position on an electric heating pad maintained at 37°C. The ring-shaped magnet on the imaging window was attached to the metal plate, which was held level to the objective lens and imaged by an upright two-photon excitation microscope. In some experiments, 20 μL of 7 mM TAK1 inhibitor 5z-7-oxozeaenol in 25% DMSO/75% PBS solution was injected under the imaging window with a 29-G needle.

**Two-photon excitation microscopy of live mice.** We used an FV1200MPE-BX61WI upright microscope (Olympus) equipped with a 25×/1.05NA water-immersion objective lens

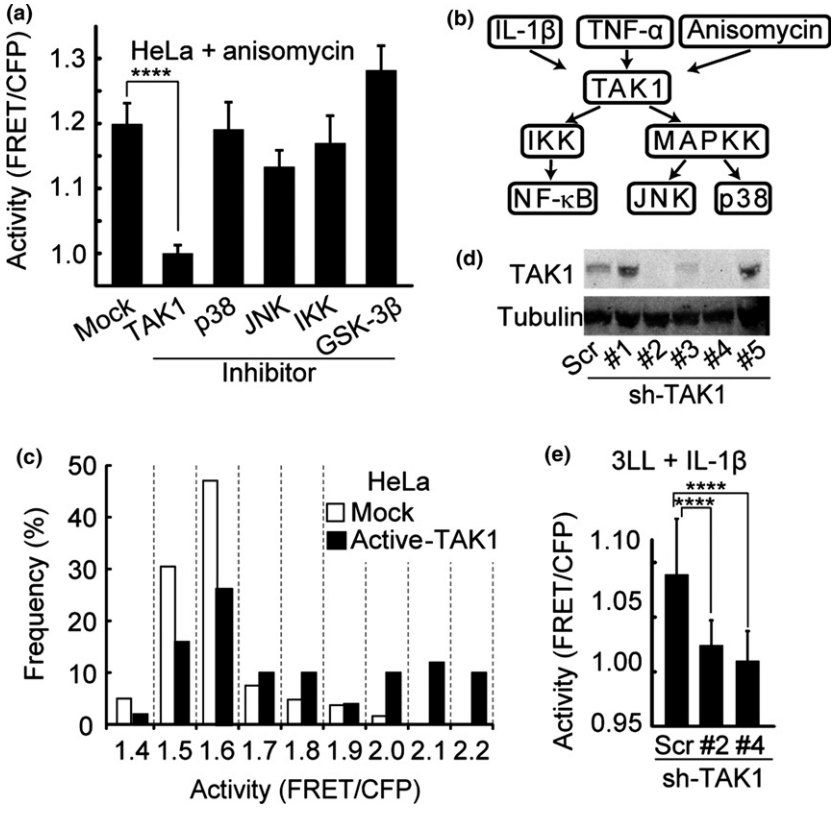


**Fig. 2.** Characterization of 3592NES as a transforming growth factor-β activated kinase 1 (TAK1) biosensor. (a) HeLa cells expressing 3592NES were time-lapse imaged without or with 3 nM (5z)-7-oxozeaenol TAK1 inhibitor, 10 μM SB203580 p38 inhibitor, 10 μM JNK inhibitor VIII, 50 μM IMD-0354 inhibitor of nuclear factor-κB (NF-κB) kinase (IKK) inhibitor, or 10 μM CHIR99021 glycogen synthase kinase-3β (GSK-3β) inhibitor. The increase in Förster resonance energy transfer/cyan fluorescent protein (FRET/CFP) was scored at 60 min after the addition of 5 μg/mL anisomycin for more than 10 cells under each condition (bars indicate SD; $^{**}P < 0.01$). (b) Flow chart of the signaling pathway of TAK1. IL-1β, interleukin 1β; TNF-α, tumor necrosis factor-α. (c) HeLa cells expressing 3592NES were mock-transfected or transfected transiently with an active-TAK1 expression vector, and examined to determine their FRET/CFP values with a fluorescent microscope. A histogram for the FRET/CFP values is shown (mock, $n = 188$; active-TAK1, $n = 81$). (d) 4T1 cells were infected with lentiviruses carrying shRNA against TAK1. Cell lysates were analyzed by immunoblotting with anti-TAK1 antibody. (e) 3592NES-expressing 3LL cells were infected with lentivirus carrying shRNA for TAK1 and stimulated with 10 ng/mL IL-1β (10 ng/mL). The increase in FRET/CFP 60 min after stimulation was scored ($n \geq 15$; $^{****}P < 0.0001$). Scr, Scramble control.

(XLPLN 25XW-MP; Olympus) for the imaging through the imaging window and an FV1000MVE inverted microscope (Olympus) equipped with a 30×/1.05NA silicon-immersion objective lens (UPLSAPO 30×S; Olympus). Both microscopes are also equipped with an InSight DeepSee Ultrafast laser (Spectra Physics, Mountain View, CA, USA), two GaAsP detector units, and two built-in photomultiplier tubes. The laser power used for observation was 10–20%. The scan speed was set at 2 μs/pixel. The excitation wavelength for CFP was 840 nm. We used an IR-cut filter, BA685RIF-3, two dichroic mirrors, DM505 and DM570, and three emission filters, BA460-500 (Olympus) for CFP, BA520-560 (Olympus) for YFP, and 645/60 (Chroma Technology Corp. Bellows Falls, VT, USA) for Alexa 647. Acquired images were analyzed with MetaMorph software (Molecular Devices) as described previously.[30]

**Statistical analysis.** *P*-values for normal distributed data were calculated with Student's *t*-test or paired Student's *t*-test for the evaluation of statistically significant differences. Otherwise, the Mann–Whitney *U*-test was used. Data analysis was carried out using Prism software (GraphPad Software, San Diego, CA, USA). $^{*}P < 0.05$; $^{**}P < 0.01$; $^{***}P < 0.001$; $^{****}P < 0.0001$.

## Results

**Response of FRET biosensor 3592NES to stress-inducing reagents.** The Eevee FRET biosensor 3592NES was originally designed to monitor GSK-3β activity in living cells. The 3592NES biosensor includes a 20-a.a. peptide derived from cyclin D1 peptide and known to be a phosphorylation site of GSK-3β (Fig. 1a). However, in our preliminary experiments, 3592NES did not respond to any GSK-3β-dependent stimuli or specific inhibitors against GSK-3β or cyclin-dependent protein kinases. During the course of characterization, however, we found that 3592NES responded markedly to anisomycin, suggesting that 3592NES may respond to stress-related kinases. In HeLa cells expressing 3592NES, anisomycin strongly increased the FRET/CFP ratio (Fig. 1b,c). Furthermore, stress-inducing cytokines, human TNF-α and mouse IL-1β, were also found to increase the FRET/CFP ratio in HeLa cells (Fig. 1c, d) and 3LL cells (Fig. 1e,f). In contrast, growth-promoting reagents such as epidermal growth factor or TPA did not increase the FRET/CFP ratio. Interestingly, the 3592NES-expressing HeLa cells responded more strongly to human TNF-α than mouse IL-1β, whereas 3LL cells responded more strongly to mouse IL-1b than human TNF-α (Fig. 1c–e). The expression of receptors for TNF-α and IL-1β in HeLa cells and 3LL cells was within a comparable range (Fig. S1A). Of note, HeLa cells were found to respond more strongly to human IL-1β than mouse IL-1β (Fig. S1B). This observation was confirmed by the immunoblotting for active p38 MAPK and JNK (Fig. S1C–E).

**Requirement of TAK1 for stimulation-induced increase in FRET/CFP of 3592NES.** To identify the kinase that phosphorylated 3592NES in response to stress-inducing stimuli, we searched for inhibitors that would abrogate the anisomycin-induced increase in FRET/CFP in 3592NES-expressing cells. Treatment with the TAK1 inhibitor, but not with other inhibitors for p38, JNK, IKK, or GSK-3β, completely suppressed the increase in FRET/CFP ratio (Fig. 2a). This result strongly suggested that 3592NES monitors TAK1 activity (Fig. 2b), or protein kinases downstream of TAK1. To confirm that 3592NES monitors TAK1 activity, we next examined the effect of an active TAK1. As TAK1 is known to be activated by binding to TAB 1, we used a TAK1–TAB 1 fusion protein as the

active-TAK1.[31] HeLa cells transfected transiently with the expression vector for active-TAK1 showed a marked increase in the fraction of cells showing a high FRET/CFP ratio in comparison with the mock-transfected cells (Fig. 2c). Next, to knockdown TAK1, we prepared five shRNAs for TAK1 and used the two shRNAs (#2 and #4) that exhibited the highest knockdown efficiency in the following experiments (Fig. 2d). Depletion of TAK1, induced by the two shRNAs, suppressed the IL-1β-stimulated increment of the FRET/CFP ratio in 3LL cells (Fig. 2e). Based on these results demonstrating that 3592NES reflects cellular TAK1 activity, we renamed 3592NES as Eevee-TAK1 and used it in the following study.

**Activation of TAK1 in 3LL cells by PolyI:C-stimulated macrophages.** With the Eevee-TAK1 biosensor in hand, we attempted to monitor the TAK1 activity of cancer cells, which are under the stress of immunological surveillance by the host. We used cells of the Lewis lung carcinoma cell line 3LL, which are known to be rejected by macrophages stimulated with double-stranded RNA analog PolyI:C.[20] The 3LL cells stably-expressing Eevee-TAK1 were imaged in the presence or absence of macrophages derived from syngeneic C57B6/L mice. The activities of TAK1 in 3LL cells showed modest heterogeneity and changed during observation (Fig. 3a). By the addition of PolyI:C to the co-culture of 3LL cells and macrophages, TAK1 activity in most 3LL cells increased within 740 min (Fig. 3b). For the precise evaluation of the effect of macrophages and PolyI:C, we randomly chose more than 60 cells and measured the FRET/CFP ratio in each condition (Fig. 3b–f). Addition of PolyI:C alone slightly increased TAK1 activity in 3LL cells (Fig. 3d). Co-culture with macrophages also increased TAK1 activity in 3LL cells within 740 min (Fig. 3e). The strongest TAK1 activation was observed when both PolyI:C was added in the presence of macrophages (Fig. 3f). This observation is consistent with the previous report showing that PolyI:C stimulates secretion of tumoricidal cytokines from macrophages.[20]

***In vivo* imaging of TAK1 activity in implanted 3LL cells.** To examine the role of TAK1 in tumor growth, 3LL carcinoma cells expressing Eevee-TAK1 were implanted into the s.c. tissue of syngeneic C57BL/6 mice and observed repeatedly through an imaging window (Fig. 4a,b). First, an imaging window consisting of a cover glass and a magnet ring was surgically implanted under the skin of a mouse hind leg. After several days, when the inflammation caused by the surgery had subsided, 3LL cells were inoculated under the imaging window. Tumors grew to approximately 2 mm in diameter within 4 days. Before image acquisition, the magnet ring of the imaging window was used to level the cover glass to the fixing implement, which minimizes motion artifacts caused by heartbeats and breathing. Then the cancer tissues were observed by an upright two-photon excitation microscope to acquire FRET images. We could clearly distinguish each tumor cell and found that 3LL cells close to the surrounding host tissues exhibited high TAK1 activity (Fig. 4c). During 5 days observation, the high TAK1 activity was confined to the cells locating at the periphery of the tumor mass. To exclude the possibility that the gradient of the FRET/CFP ratio in the tumor tissue was an artifact, we used 3LL cells expressing a negative control FRET biosensor AKAREV-NC, in which the phosphorylation site of the FRET biosensor was

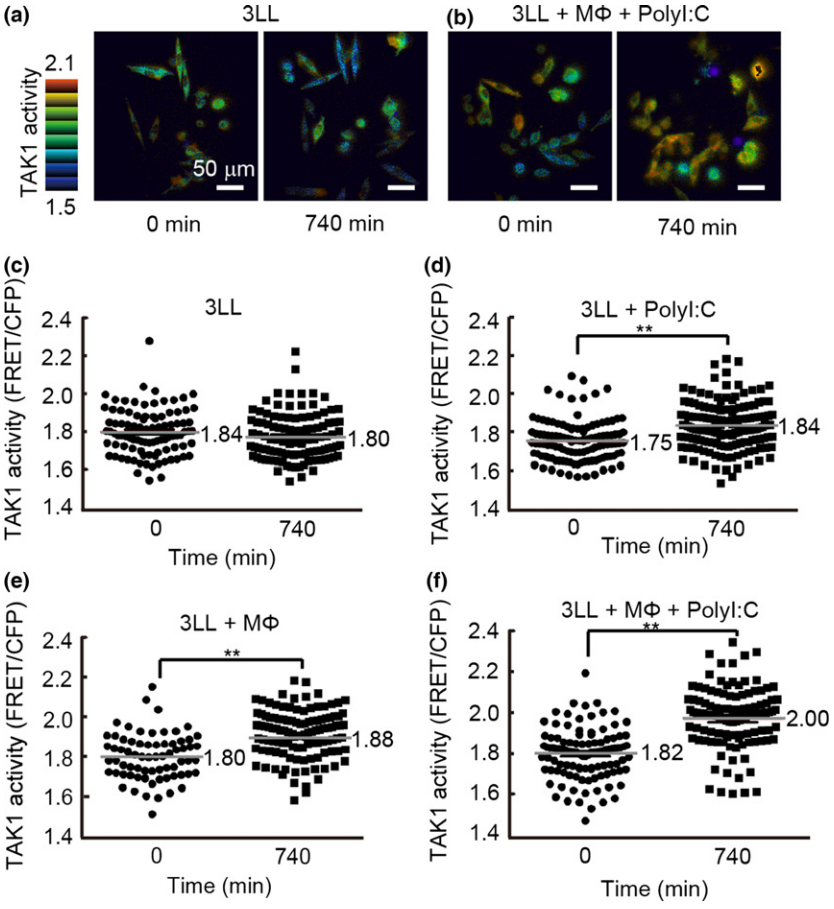


**Fig. 3.** Activation of transforming growth factor-b activated kinase 1 (TAK1) by polyinosinic: polycytidylic acid (polyI:C)-stimulated macrophages. 3LL cells expressing 3592NES were cultured alone (a, c). 3LL cells expressing 3592NES with 50 μg/mL PolyI:C (d), or cocultured with macrophages (MΦ) in the absence (e) or presence (b, f) of PolyI:C. Cells were imaged under an epifluorescence microscope (scale bar = 50 μm) and quantified for Förster resonance energy transfer/cyan fluorescent protein ($n \geq 60$; $^{**}P < 0.01$).

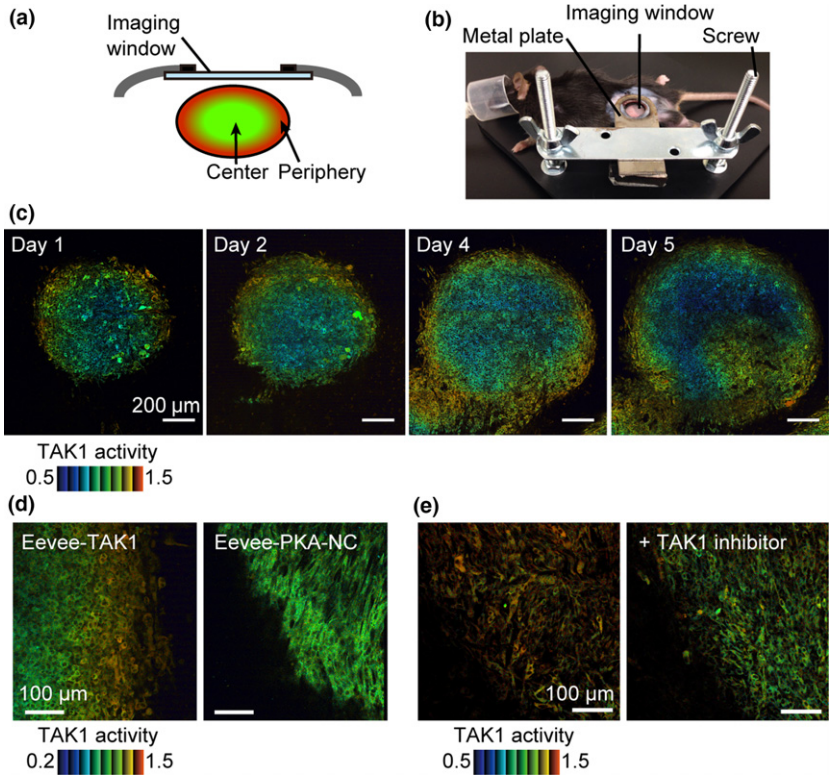


**Fig. 4.** Intravital imaging of transforming growth factor-β activated kinase 1 (TAK1) activity in an allograft model of Lewis lung carcinoma. (a) Schematic view of the imaging window consisting of a cover glass and a magnet ring. Several days after the operation, 3LL cells were inoculated under the imaging window. (b) The magnet ring of the imaging window was used to level the cover glass to the fixing implement, which minimizes motion artifacts caused by heartbeats and breathing. (c) 3LL cells expressing the TAK1 biosensor 3592NES were observed by an upright two-photon excitation microscope to acquire Förster resonance energy transfer (FRET) images. From 4 days after inoculation, the same tumor was observed at days 1, 2, 4, and 5. (d) 3LL cells expressing 3592NES and a negative control FRET biosensor AKAREV-NC (PKA-NC) were observed under the same imaging conditions. Similar results were obtained in three independent experiments. (e) 3LL cells expressing 3592NES were inoculated as described and imaged before and 1 h after injection of TAK1 inhibitor (5z)-7-oxozeaenol.

substituted with alanine.[30] As shown in Figure 4(d), the 3LL cells expressing AKAREV-NC did not show a remarkable gradient in the FRET/CFP ratio. To confirm that the high FRET/CFP ratio in the tumor tissue reflected TAK1 activity, TAK1 inhibitor (5z)-7-oxozeaenol was injected below the imaging window (Fig. 4e). As expected, the TAK1 inhibitor robustly decreased the FRET/CFP ratio.

**Polyinosinic:polycytidylic acid-induced TAK1 activation *in vivo*.** Activation of innate immunity mediated by PolyI:C is known to induce the regression of 3LL cells in a syngeneic transplantation model. Therefore, we next examined the effect of PolyI:C on TAK1 activity. Twenty-four hours after injection, TAK1 activity was robustly elevated in almost all cells within the tumor tissue including the 3LL cells located at the periphery (Fig. 5a,b). Interestingly, a quantity of 3LL cells at the border of tumor tissues showed marked changes in shape: the round 3LL cells became spindle-shaped, extended cellular processes, and appeared to have begun invading into the surrounding tissues; these are all typical morphological changes of EMT, therefore EMT might have occurred (Fig. 5c). The high TAK1 activity subsided within 4 days to restore the original morphology and gradient of TAK1 activity. Notably, the second PolyI:C injection induced TAK1 activation again, indicating that the decrease of TAK1 activity on day 4 was caused by the decrease of PolyI:C in the tissue, rather than by the adaptation of tumor cells to PolyI:C (Fig. 5a).

Polyinosinic:polycytidylic acid is thought to cause tumor necrosis through cytokines secreted from myeloid-derived cells among the tumor cells. We speculated that the enrichment of the myeloid-derived cells at the periphery of the tumor mass may have caused the TAK1 activity gradient in the tumor tissue. To visualize the localization of the myeloid-derived cells in and around the allograft, we injected Alexa Fluor 647 anti-mouse F4/80 antibody, a marker for mature macrophages and monocytes, into the tumors in the absence of PolyI:C. The F4/80-positive cells were distributed in and around the tumor, negating the possibility that the gradient of TAK1 activity in the tumor reflected the localized recruitment of myeloid cells (Fig. 5d).

## Discussion

In this study, we developed Eevee-TAK1, a new FRET-based biosensor monitoring TAK1 activity in living cells, and detected TAK1 activity at single-cell resolution. With Eevee-TAK1, we found that TAK1 activity was significantly higher in 3LL cells locating at the periphery of the tumor than in 3LL cells locating at the center of the tumor (Fig. 4c). Because TAK1 responds to inflammatory stresses,[6–8] we speculated that inflammatory cytokines or direct interaction with antitumor immune cells caused TAK1 activation in the tumor cells locating at the periphery of the tumor. However, against our expectation, F4/80-positive macrophages were observed diffusely in the tumor tissues (Fig. 5c). It is still possible that macrophages surrounding the tumor cells are more active than the macrophages within the tumor cells, which should be examined in a future study.

The high level of TAK1 activity in the peripheral tumor cells is reasonable if we consider the positive role of TAK1 in EMT.[2,3] In agreement with this reasoning, we found that PolyI:C treatment causes significant TAK1 activation and EMT-like morphological changes of 3LL tumor cells at the periphery of the tumor cells (Fig. 5b). However, in our preliminary experiments, we failed to detect the induction of EMT markers such as E-cadherin, α-smooth muscle actin, Snail, or vimentin. Therefore, it is currently unknown whether the high

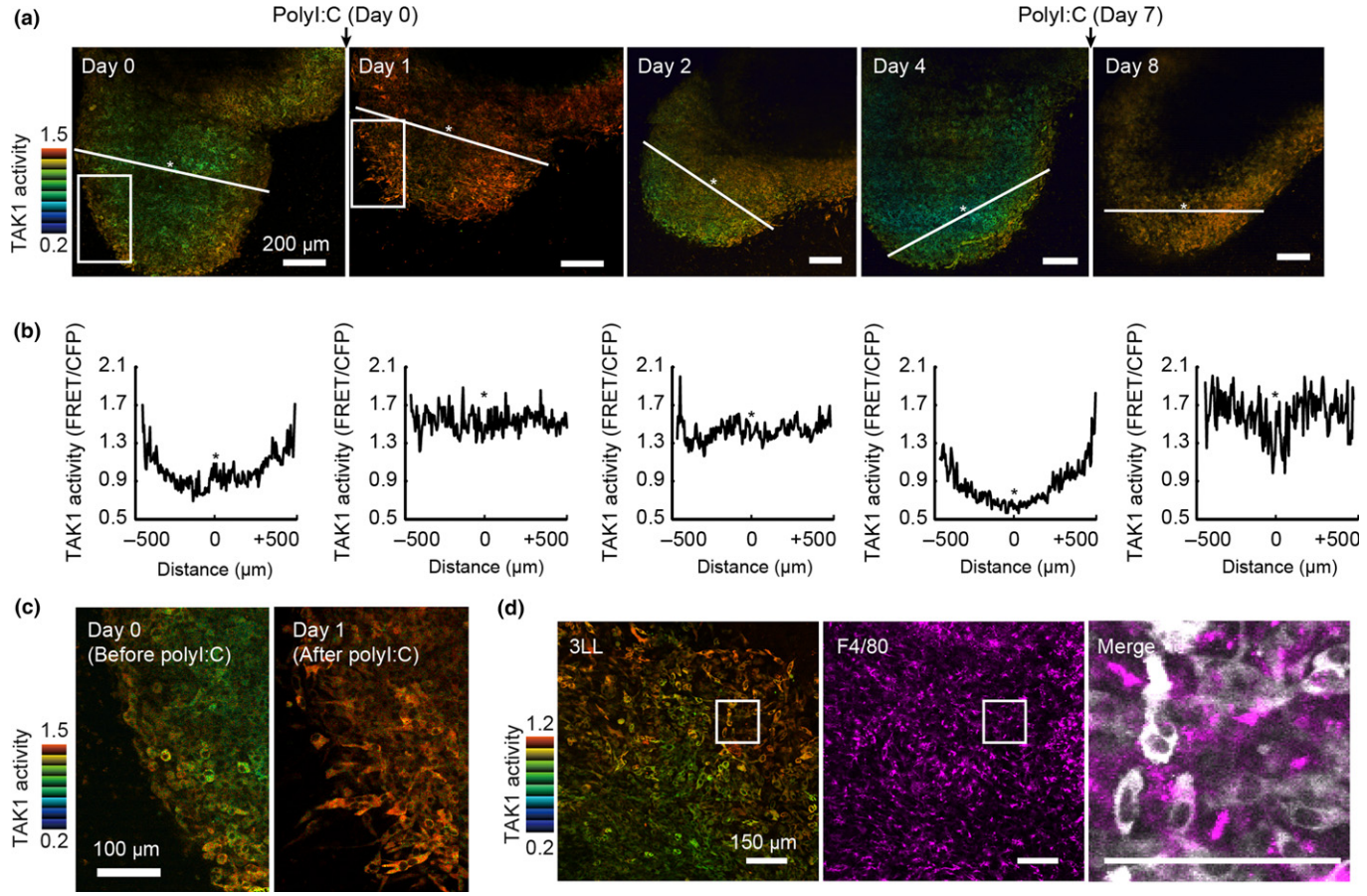


**Fig. 5.** Polyinosinic:polycytidylic acid (PolyI:C)-induced transforming growth factor-β activated kinase 1 (TAK1) activation *in vivo*. 3LL Lewis lung carcinoma cells expressing 3592NES were implanted below the imaging window. (a) Förster resonance energy transfer (FRET) images from days 0 to 8. Subcutaneous injection of 200 μg PolyI:C was carried out on day 0, just after image acquisition, and day 7. (b) FRET/cyan fluorescent protein ratio was plotted along the white lines in (a). Asterisks indicate the origin. (c) Regions marked by white boxes in (a) are enlarged to show PolyI:C-induced morphological changes. (d) Macrophages beneath the window were marked with Alexa Fluor 647 anti-mouse F4/80 antibody. Right panel, merged image of white-boxed regions.

TAK1 activity at the peripheral region of the tumor is related to EMT.

Phosphorylation of $Thr^{286}$ of cyclin D1 plays a critical role in its cell cycle-dependent degradation.[32,33] Originally, GSK-3β was believed to be responsible for $Thr^{286}$ phosphorylation, but a later study showed that the checkpoint kinases ATR and ATM primarily phosphorylate $Thr^{286}$ during the cell cycle.[34] More recently, DYRKs have also been shown to phosphorylate cyclin D1 on $Thr^{286}$ and regulate the cell cycle.[35,36] We failed to detect cell cycle-dependent changes in the FRET signal in HeLa cells expressing the TAK1 biosensor (data not shown). Moreover, none of the inhibitors against GSK-3β, ATM/ATR, and DYRKs suppressed the anisomycin- or TNF-α-induced increase in the FRET signal of the 3592NES TAK1 biosensor. Nevertheless, we should keep in mind that these observations do not negate the possibility that GSK-3β, ATM/ATR, and DYRKs may contribute the FRET signal in the TAK1 biosensor-expressing cells under different conditions.

One of the most difficult tasks in the development of a FRET biosensor for a protein kinase is the selection of a substrate peptide that is specific to the protein kinase of interest. With the ongoing progress in phospho-proteomics, more than 100 000 human protein phosphorylation sites are now deposited in PhosphoSitePlus and other databases.[37] Recently, substrate databases of protein kinases have also been constructed by a novel method named KISS.[38] These bidirectional approaches will help identify the consensus phosphorylation sequence of each protein kinase, which in turn will assist in the development of FRET biosensors for protein kinases. Although a consensus phosphorylation sequence of TAK1 was reported previously, most of the known substrates did not match this consensus sequence (Table S1). Therefore, it remains unknown why the amino acid sequence encompassing $Thr^{286}$ of cyclin D1 served as an effective sensor for TAK1 activity. Moreover, in our experience, most of the reported consensus sequences for the protein kinases were not sufficiently specific for the individual kinases. For example, in the case of the FRET biosensor for ERK and JNK, in addition to the consensus phosphorylation sequences, docking sequences are required for the endowment of specificity to the biosensors.[39,40] Therefore, the cyclin D1 sequence used in Eevee-TAK1 may coincidentally include the docking sequence to TAK1.

In conclusion, by using our newly developed TAK1 biosensor and an imaging window for *in vivo* imaging, the states of stress in tumor cells could be visualized for several days or more. This technique should open a new window onto the spatiotemporal effects of antitumor drugs during the induction of tumor necrosis.

## Acknowledgments

We thank Kosuke Yusa, Allan Bradly, Hiroaki Sakurai, Tohru Ishitani, and Kunihiro Matsumoto for the plasmids, and the members of the Matsuda Laboratory for their technical assistance. This work was supported by the Platform Project for Supporting Drug Discovery and Life Science Research (Platform for Dynamic Approaches to Living System) of the Ministry of Education, Culture, Sports, and Science of Japan, by the Japan Agency for Medical Research and Development, by the Innovative Techno-Hub for Integrated Medical Bio-imaging Project of the Special Coordination Funds for Promoting Science and Technology, and by a Japan Society for the Promotion of Science KAKENHI Grant-in-Aid for Young Scientists (B) 23701053 and 26830070.

## Disclosure Statement

The authors have no conflict of interest.

## Abbreviations

| | |
|---|---|
| a.a. | amino acid |
| ATM | ataxia-telangiectasia mutated |
| ATR | ATM and RAD3-related |
| CFP | cyan fluorescent protein |
| DYRK | dual-specificity tyrosine phosphorylation-regulated kinase |
| EMT | epithelial mesenchymal transition |
| IL-1β | interleukin 1-β |
| GSK-3β | glycogen synthase kinase-3β |
| NES | nuclear export signal |
| PolyI:C | polyinosinic:polycytidylic acid |
| TAB1 | TAK1-binding protein 1 |
| TAK1 | TGF-β activated kinase 1 |
| TGF-β | transforming growth factor-β |
| TNF-α | tumor necrosis factor-α |

## References

1 Yamaguchi K, Shirakabe T, Shibuya H *et al.* Identification of a member of the MAPKKK family as a potential mediator of TGF-beta signal transduction. *Science* 1995; **270**: 2008–11.
2 Yamashita M, Fatyol K, Jin C, Wang X, Liu Z, Zhang YE. TRAF6 mediates Smad-independent activation of JNK and p38 by TGF-beta. *Mol Cell* 2008; **31**: 918–24.
3 Sorrentino A, Thakur N, Grimsby S *et al.* The type I TGF-beta receptor engages TRAF6 to activate TAK1 in a receptor kinase-independent manner. *Nat Cell Biol* 2008; **10**: 1199–207.
4 Sakurai H, Miyoshi H, Toriumi W, Sugita T. Functional interactions of transforming growth factor beta-activated kinase 1 with IkappaB kinases to stimulate NF-kappaB activation. *J Biol Chem* 1999; **274**: 10641–8.
5 Ninomiya-Tsuji J, Kishimoto K, Hiyama A, Inoue J, Cao Z, Matsumoto K. The kinase TAK1 can activate the NIK-I kappaB as well as the MAP kinase cascade in the IL-1 signalling pathway. *Nature* 1999; **398**: 252–6.
6 Hayden MS, Ghosh S. Shared principles in NF-kappaB signaling. *Cell* 2008; **132**: 344–62.
7 Sakurai H. Targeting of TAK1 in inflammatory disorders and cancer. *Trends Pharmacol Sci* 2012; **33**: 522–30.
8 Mihaly SR, Ninomiya-Tsuji J, Morioka S. TAK1 control of cell death. *Cell Death Differ* 2014; **21**: 1667–76.
9 Sato S, Sanjo H, Takeda K *et al.* Essential function for the kinase TAK1 in innate and adaptive immune responses. *Nat Immunol* 2005; **6**: 1087–95.
10 Shim JH, Xiao C, Paschal AE *et al.* TAK1, but not TAB 1 or TAB 2, plays an essential role in multiple signaling pathways in vivo. *Genes Dev* 2005; **19**: 2668–81.
11 Wan YY, Chi H, Xie M, Schneider MD, Flavell RA. The kinase TAK1 integrates antigen and cytokine receptor signaling for T cell development, survival and function. *Nat Immunol* 2006; **7**: 851–8.
12 Omori E, Matsumoto K, Sanjo H *et al.* TAK1 is a master regulator of epidermal homeostasis involving skin inflammation and apoptosis. *J Biol Chem* 2006; **281**: 19610–7.
13 Morioka S, Broglie P, Omori E *et al.* TAK1 kinase switches cell fate from apoptosis to necrosis following TNF stimulation. *J Cell Biol* 2014; **204**: 607–23.
14 Grivennikov SI, Greten FR, Karin M. Immunity, inflammation, and cancer. *Cell* 2010; **140**: 883–99.
15 Condeelis J, Pollard JW. Macrophages: obligate partners for tumor cell migration, invasion, and metastasis. *Cell* 2006; **124**: 263–6.
16 Balkwill F. Tumour necrosis factor and cancer. *Nat Rev Cancer* 2009; **9**: 361–71.
17 Safina A, Ren MQ, Vandette E, Bakin AV. TAK1 is required for TGF-beta 1-mediated regulation of matrix metalloproteinase-9 and metastasis. *Oncogene* 2008; **27**: 1198–207.
18 Choo MK, Sakurai H, Koizumi K, Saiki I. TAK1-mediated stress signaling pathways are essential for TNF-alpha-promoted pulmonary metastasis of murine colon cancer cells. *Int J Cancer* 2006; **118**: 2758–64.
19 Singh A, Sweeney MF, Yu M *et al.* TAK1 inhibition promotes apoptosis in KRAS-dependent colon cancers. *Cell* 2012; **148**: 639–50.
20 Shime H, Matsumoto M, Oshiumi H *et al.* Toll-like receptor 3 signaling converts tumor-supporting myeloid cells to tumoricidal effectors. *Proc Natl Acad Sci USA* 2012; **109**: 2066–71.
21 Sample V, Mehta S, Zhang J. Genetically encoded molecular probes to visualize and perturb signaling dynamics in living biological systems. *J Cell Sci* 2014; **127**: 1151–60.
22 Miyawaki A, Niino Y. Molecular spies for bioimaging-fluorescent protein-based probes. *Mol Cell* 2015; **58**: 632–43.
23 Aoki K, Komatsu N, Hirata E, Kamioka Y, Matsuda M. Stable expression of FRET biosensors: a new light in cancer research. *Cancer Sci* 2012; **103**: 614–9.
24 Yukinaga H, Shionyu C, Hirata E *et al.* Fluctuation of Rac1 activity is associated with the phenotypic and transcriptional heterogeneity of glioma cells. *J Cell Sci* 2014; **127**: 1805–15.
25 Hirata E, Girotti MR, Viros A *et al.* Intravital imaging reveals how BRAF inhibition generates drug-tolerant microenvironments with high integrin beta1/FAK signaling. *Cancer Cell* 2015; **27**: 574–88.
26 Komatsu N, Aoki K, Yamada M *et al.* Development of an optimized backbone of FRET biosensors for kinases and GTPases. *Mol Biol Cell* 2011; **22**: 4647–56.
27 Sakurai H, Nishi A, Sato N, Mizukami J, Miyoshi H, Sugita T. TAK1-TAB 1 fusion protein: a novel constitutively active mitogen-activated protein kinase kinase kinase that stimulates AP-1 and NF-kappaB signaling pathways. *Biochem Biophys Res Commun* 2002; **297**: 1277–81.
28 Moffat J, Grueneberg DA, Yang X *et al.* A lentiviral RNAi library for human and mouse genes applied to an arrayed viral high-content screen. *Cell* 2006; **124**: 1283–98.
29 Aoki K, Matsuda M. Visualization of small GTPase activity with fluorescence resonance energy transfer-based biosensors. *Nat Protoc* 2009; **4**: 1623–31.
30 Kamioka Y, Sumiyama K, Mizuno R *et al.* Live imaging of protein kinase activities in transgenic mice expressing FRET biosensors. *Cell Struct Funct* 2012; **37**: 65–73.
31 Yusa K, Rad R, Takeda J, Bradley A. Generation of transgene-free induced pluripotent mouse stem cells by the piggyBac transposon. *Nat Methods* 2009; **6**: 363–9.
32 Diehl JA, Cheng M, Roussel MF, Sherr CJ. Glycogen synthase kinase-3beta regulates cyclin D1 proteolysis and subcellular localization. *Genes Dev* 1998; **12**: 3499–511.
33 Guo Y, Yang K, Harwalkar J *et al.* Phosphorylation of cyclin D1 at Thr 286 during S phase leads to its proteasomal degradation and allows efficient DNA synthesis. *Oncogene* 2005; **24**: 2599–612.
34 Hitomi M, Yang K, Stacey AW, Stacey DW. Phosphorylation of cyclin D1 regulated by ATM or ATR controls cell cycle progression. *Mol Cell Biol* 2008; **28**: 5478–93.
35 Ashford AL, Oxley D, Kettle J *et al.* A novel DYRK1B inhibitor AZ191 demonstrates that DYRK1B acts independently of GSK3beta to phosphorylate cyclin D1 at Thr(286), not Thr(288). *Biochem J* 2014; **457**: 43–56.
36 Soppa U, Schumacher J, Florencio Ortiz V, Pasqualon T, Tejedor FJ, Becker W. The Down syndrome-related protein kinase DYRK1A phosphorylates p27(Kip1) and Cyclin D1 and induces cell cycle exit and neuronal differentiation. *Cell Cycle* 2014; **13**: 2084–100.
37 Hornbeck PV, Kornhauser JM, Tkachev S *et al.* PhosphoSitePlus: a comprehensive resource for investigating the structure and function of experimentally determined post-translational modifications in man and mouse. *Nucleic Acids Res* 2012; **40**: D261–70.
38 Amano M, Hamaguchi T, Shohag MH *et al.* Kinase-interacting substrate screening is a novel method to identify kinase substrates. *J Cell Biol* 2015; **209**: 895–912.

39 Fosbrink M, Aye-Han NN, Cheong R, Levchenko A, Zhang J. Visualization of JNK activity dynamics with a genetically encoded fluorescent biosensor. *Proc Natl Acad Sci USA* 2010; **107**: 5459–64.

40 Harvey CD, Ehrhardt AG, Cellurale C *et al.* A genetically encoded fluorescent sensor of ERK activity. *Proc Natl Acad Sci USA* 2008; **105**: 19263–8.

## Supporting Information

Additional Supporting Information may be found online in the supporting information tab for this article:

**Fig. S1.** Detection of species-specific responses to tumor necrosis factor-α (TNF-α) and interleukin-1β (IL-1β).

**Table S1.** Consensus phosphylation sequence of transforming growth factor-β activated kinase 1 (TAK1).